Extended isogeometric boundary element method (XIBEM) for three-dimensional medium-wave acoustic scattering problems

M.J. Peake, J. Trevelyan*, G. Coates

Durham University, School of Engineering and Computing Sciences, Durham, DH1 3LE, United Kingdom

Abstract

A boundary element method (BEM), based on non-uniform rational B-splines (NURBS), is used to find solutions to three-dimensional wave scattering problems governed by the Helmholtz equation. The method is extended in a partition-of-unity sense, multiplying the NURBS functions by families of plane waves; this method is called the eXtended Isogeometric Boundary Element Method (XIBEM).

In this paper, the collocation XIBEM formulation is described and numerical results given. The numerical results are compared against closed-form or converged solutions. Comparisons are made against the conventional boundary element method and the non-enriched isogeometric BEM (IGABEM).

When compared to non-enriched boundary element simulations, using XIBEM significantly reduces the number of degrees of freedom required to obtain a solution of a given error; thus, with a fixed computational resource, problems of a shorter wavelength can be solved.

*Corresponding author

Email address: jon.trevelyan@durham.ac.uk (J. Trevelyan)

Keywords: Helmholtz, acoustics, wave scattering, isogeometric analysis, boundary element method, partition of unity

1. Introduction

The boundary element method (BEM) is a popular technique for finding solutions to exterior problems governed by the Helmholtz equation. The reasons for this include the BEM's inherent ability to model infinite domains without the need for artificial boundary conditions or domain truncation. The method is also popular because scatterers need only to have their boundary meshed, rather than the complete volume. This reduction of dimensionally makes mesh generation a simpler process than with alternative techniques like the finite element method.

Early development of the BEM for acoustics can be traced back to the 1960s and the work of Banaugh and Goldsmith [1] and Copley [2]. This early work uncovered a non-uniqueness problem that arises when solving exterior problems at discrete eigenfrequencies associated with the corresponding interior Dirichlet problem. Two common methods of overcoming this are the CHIEF [3] and the Burton-Miller formulation [4].

Much of the recent research into the BEM has been focused on short-wave problems. Bettess [5] describes such problems as those 'in which the wavelength is much smaller than any other parameters in the problem'. Numerical analysis of wave phenomena requires a modelling technique capable of reproducing oscillations. A commonly applied heuristic dictates that conventional BEM approaches require 10 degrees of freedom per wavelength in each coordinate direction in order to effectively capture wave oscillations and

obtain an 'engineering accuracy' ($\sim 1\%$). A result of this is that the computational efficiency of BEM analysis of wave problems is strongly dependent on the wavelength, λ, of such waves: for a three dimensional problem, the number of BEM degrees of freedom required is proportional to λ^{-2}.

Consider a 10 GHz radar wave being scattered by an aircraft—the wave has a wavelength of 0.03 metres (relatively large for radar). Say the aircraft has a surface area of approximately 1,250 square metres or 1.4×10^6 square wavelengths. This equates to 140×10^6 nodal variables leading to a matrix system with 19×10^{15} entries. Clearly, even for this medium-wave problem, it is imperative to find a way to reduce the nodal spacing requirement of these simulations: enriched methods may offer a solution.

The partition-of-unity method, introduced by Bubuška and Melenk [6], is a general framework for enriching the approximation space by including, in the basis, some functions that have better approximation properties (for the PDE at hand) than piecewise polynomials. For Helmholtz problems, this is commonly achieved by the use of plane waves. Initially developed for finite elements, this approach has been applied to the Galerkin BEM [7] and collocation BEM [8]; the latter work demonstrated a significant reduction in the degrees of freedom required compared to a conventional BEM scheme. The partition-of-unity method has also been used successfully for shortwave problems in [9–11].

In general computational engineering research, there have been attempts to integrate computer-aided design (CAD) by taking spline-based CAD geometries and using them directly in numerical analysis; this approach is known as isogeometric analysis (IGA) [12]. The primary advantage of using

boundary elements for IGA (a combination referred to as IGABEM) is that the functions used in CAD describe only the boundary. It appears that BEM and CAD could be fully integrated. Finite element meshes can be also formed from CAD descriptions but it is a considerably more complex process.

While IGA may be a relatively new term, the concept of using splines in BEM is not. In 1990, Cabral *et al.* [13, 14] presented a BEM formulation using B-splines for problems governed by Laplace's equation. An isoparametric formulation was used and it was concluded that these functions were well-suited to solve BEM problems.

More recently, research under the name of isogeometric BEM is increasing rapidly: Politis *et al.* [15] presented an isogeometric BEM for problems of potential flow; Kang and Qian [16] have presented an isogeometric boundary integral method for shape optimization; Simpson *et al.* [17, 18] applied the approach to elastostatic analysis, coining the term IGABEM; Takahashi and Matsumoto [19] applied the fast multipole method to IGABEM for the Laplace equation; Scott *et al.* [20] employed T-splines for elastostatic problems; Belibassakisa *et al.* [21] presented an isogeometric BEM method for the ship wave resistance problem; and Heltai *et al.* [22] solved Stokes flow problems in 3D with IGABEM.

Some research has already been conducted in the field of isogeometric boundary elements for acoustic problems by Simpson *et al.* [23]. The results showed IGABEM to have superior accuracy compared to conventional BEM schemes. However, the number of degrees of freedom required to solve a specific problem to a given accuracy is still governed by the nodal spacing heuristic used for piecewise polynomial approximation spaces. A combined

approach benefits from simple meshing, exact geometry and enriched approximation spaces. To this end, the eXtended Isogeometric Boundary Element Method (XIBEM) was developed by the current authors for two-dimensional acoustic scattering problems [24]. XIBEM simulations outperformed IGA-BEM simulations by using fewer degrees of freedom and providing solutions of a greater accuracy.

This paper focuses on developing a collocation XIBEM for three-dimensional acoustic scattering problems. Section 2 gives a brief overview of the required theory for the new approach; Section 3 shows some numerical results relating to two problems (the unit sphere and torus); Section 4 discusses these results and draws some conclusions.

2. Formulation of XIBEM for the Helmholtz equation

2.1. Boundary integral equation

An infinite acoustic domain $\Omega \subset \mathbb{R}^3$ contains a smooth scatterer of boundary $\Gamma := \partial\Omega$. Acoustic waves within Ω are governed by the wave equation which, assuming $\exp(-\iota\omega t)$ time dependence where ω is angular velocity, is reduced to the homogeneous Helmholtz equation:

$$\nabla^2\phi(\mathbf{p}) + k^2\phi(\mathbf{p}) = 0, \quad \mathbf{p} \in \Omega, \tag{1}$$

where ∇^2 is the Laplacian operator, $\phi \in \mathbb{C}$ is the wave potential, and k is the wavenumber ($\lambda = 2\pi/k$ is the wavelength). For scattering problems, an exterior incident wave is defined; in this work, the scatterer is impinged by a plane wave,

$$\phi^{\text{inc}}(\mathbf{p}) = A^{\text{inc}} \exp(\iota k \mathbf{d}^{\text{inc}} \cdot \mathbf{p}), \quad \left|\mathbf{d}^{\text{inc}}\right| = 1, \tag{2}$$

where $A^{\text{inc}} \in \mathbb{C}$ is the wave's amplitude and $\mathbf{d}^{\text{inc}}$ is its direction of propagation.

To obtain the boundary integral equation (BIE), many authors use Green's second identity and the Green's function for (1), a technique documented in [25] and a number of other texts. The process yields

$$c(\mathbf{p})\phi(\mathbf{p}) = \int_\Gamma \left[G(\mathbf{p},\mathbf{q}) \frac{\partial \phi(\mathbf{q})}{\partial n(\mathbf{q})} - \frac{\partial G(\mathbf{p},\mathbf{q})}{\partial n(\mathbf{q})} \phi(\mathbf{q}) \right] \mathrm{d}\Gamma(\mathbf{q}) + \phi^{\text{inc}}(\mathbf{p}), \quad \mathbf{p},\mathbf{q} \in \Gamma, \quad (3)$$

where n is a unit-normal pointing outward of Ω (i.e. into the scatterer) and, assuming Γ is smooth, the jump term $c(\mathbf{p}) = 1/2$. $G(\mathbf{p},\mathbf{q})$ is the Green's function, representing the field effect experienced at $\mathbf{q}$ from a unit-source at $\mathbf{p}$; in three-dimensional space it is

$$G(\mathbf{p},\mathbf{q}) = \frac{e^{ikr}}{4\pi r}, \quad (4)$$

where $r = |\mathbf{p} - \mathbf{q}|$.

2.1.1. Boundary conditions

In the current work, a solution to (1) is sought, subject to the general Robin boundary condition,

$$\frac{\partial \phi(\mathbf{q})}{\partial n(\mathbf{q})} = \alpha(\mathbf{q})\phi(\mathbf{q}) + \beta(\mathbf{q}), \quad \mathbf{q} \in \Gamma. \quad (5)$$

$\beta \in \mathbb{C}$ is non-zero for active boundary conditions (radiation problems) and zero otherwise; $\alpha \in \mathbb{C}$ is an impedance property of the scatterer. The sub-

stitution of (5) into (3) and a small rearrangement yields

$$c(\mathbf{p})\phi(\mathbf{p}) + \int_\Gamma \left[\frac{\partial G(\mathbf{p},\mathbf{q})}{\partial n(\mathbf{q})} - \alpha(\mathbf{q})G(\mathbf{p},\mathbf{q})\right]\phi(\mathbf{q})\mathrm{d}\Gamma(\mathbf{q}) = \int_\Gamma \beta(\mathbf{q})G(\mathbf{p},\mathbf{q})\mathrm{d}\Gamma(\mathbf{q}) + \phi^{\mathrm{inc}}(\mathbf{p}), \quad \mathbf{p},\mathbf{q}\in\Gamma. \quad (6)$$

2.1.2. Regularisation

Before discretising this equation, one should first consider the different types of Green's functions within the integrals. Both of the integrals in (6) are weakly-singular, requiring care when r is small. While coordinate transformations exist, it is worth considering the use of a regularisation scheme.

Several regularisation schemes exist that remove the singularity of the derivative Green's function $\partial G/\partial n$. The regularised BIE described below, adapted from Liu [26], makes use of the derivative of the Green's function, $\bar{G}$, for the Laplace equation:

$$\frac{\partial \bar{G}(\mathbf{p},\mathbf{q})}{\partial n} = -\frac{1}{4\pi r^2}\frac{\partial r}{\partial n}. \quad (7)$$

Liu's regularisation is derived from the ability to express the jump term $c(\mathbf{p})$ as

$$c(\mathbf{p}) = 1 - \int_\Gamma \frac{\partial \bar{G}(\mathbf{p},\mathbf{q})}{\partial n(\mathbf{q})}\mathrm{d}\Gamma(\mathbf{q}), \quad \forall \mathbf{p}\in\Gamma, \quad (8)$$

The jump term (8) can be substituted into a rearranged (6) to obtain the regularised BIE (RBIE):

$$\phi(\mathbf{p}) + \int_\Gamma \frac{\partial \bar{G}(\mathbf{p},\mathbf{q})}{\partial n(\mathbf{q})}\left[\phi(\mathbf{q}) - \phi(\mathbf{p})\right]\mathrm{d}\Gamma(\mathbf{q}) + \int_\Gamma \left[\frac{\partial G(\mathbf{p},\mathbf{q})}{\partial n(\mathbf{q})} - \alpha(\mathbf{q})G(\mathbf{p},\mathbf{q}) - \frac{\partial \bar{G}(\mathbf{p},\mathbf{q})}{\partial n(\mathbf{q})}\right]\phi(\mathbf{q})\mathrm{d}\Gamma(\mathbf{q}) = \int_\Gamma \beta(\mathbf{q})G(\mathbf{p},\mathbf{q})\mathrm{d}\Gamma(\mathbf{q}) + \phi^{\mathrm{inc}}(\mathbf{p}), \quad \mathbf{p},\mathbf{q}\in\Gamma. \quad (9)$$

In the second integral of (9), one can see that the the Laplace derivative Green's function is subtracted from the Helmholtz derivative Green's function. As $G(p,q) \to \bar{G}(p,q)$ as $r \to 0$, the Laplace derivative Green's function is effectively removing that singularity from the integral. In the first integral, while $\partial\bar{G}/\partial n$ is singular, $\phi(\mathbf{q}) - \phi(\mathbf{p}) \to 0$ as $\mathbf{q} \to \mathbf{p}$ (the point of singularity). The derivative Green's function for the Laplace equation is $\mathcal{O}(1/r)$ and the regularising term is $\mathcal{O}(r)$; hence, the product of the two terms is $\mathcal{O}(1)$ (regular).

The Green's function for the Helmholtz equation, $G(\mathbf{p},\mathbf{q})$, is still weakly singular and requires treatment by way of a coordinate transformation such as [27]; however, for problems of perfectly reflecting scatterers ($\alpha = \beta = 0$), the regularisation scheme above is more effective than a coordinate transformation.

2.2. IGABEM

Conventional BEM approaches use Lagrangian shape functions to approximate both the geometry of Γ and the unknown functional variables. IGABEM uses the functions that describe geometries in CAD for this purpose. While there is an increasing amount of IGA research into T-splines [20, 28], non-uniform rational B-splines (NURBS) are still ubiquitous in CAD software. For this reason, NURBS functions are adopted in the current work for the geometry and function representations. A comprehensive introduction to the subject of NURBS is given in [29].

It is desirable to decompose the NURBS surface into its component Bézier patches—a process known as Bézier decomposition. This allows the NURBS surface to be considered as a set of piecewise elements (as in a conventional

BEM approach); Bézier patches are also more computationally efficient to use compared to NURBS surfaces. The process of decomposition is somewhat similar to Bézier extraction described in [30].

It should be noted that the motivation to use Bézier decomposition is primarily as it provides a set of C^0 patches that can be easily implemented into existing BEM codes that use Lagrangian elements. However, it should be noted that this process can involve the insertion of unnecessary control points and basis functions that removes the smoothness of the original NURBS surface; this is particularly true for high-order NURBS surfaces. A code written specifically for isogeometric analysis would ideally not use Bézier decomposition. However, it will be shown that the enrichment used in XIBEM has a much more significant impact on accuracy than the mesh refinement or smoothness.

2.2.1. Discretisation

To simplify the description of the method, it is assumed that the scatterer boundary can be expressed as a single NURBS surface, Γ. This surface is decomposed into E non-overlapping elements (rational Bézier patches) of order p. The analytical geometry on each element Γ_e is given by

$$\Gamma_e = \{\mathbf{F}_e(\xi_1, \xi_2) : \xi_1, \xi_2 \in [0, 1)\}, \quad e = 1, \ldots, E, \tag{10}$$

where $\mathbf{F}_e : \mathbb{R}^2 \to \mathbb{R}^3$ is a mapping using the rational Bézier functions that are used for the geometry representation. The variation of potential, ϕ, over Γ_e is also mapped using $\mathbf{F}_e$; this can be formally expressed as,

$$\phi^e(\mathbf{q}_\xi) = \sum_{i=0}^{p} \sum_{j=0}^{p} R_{ij}^e(\xi_1, \xi_2) \bar{\phi}_{ij}^e, \tag{11}$$

where $\mathbf{q}_\xi \equiv \mathbf{q}(\xi_1, \xi_2)$, the element consists of a $(p+1) \times (p+1)$ grid of *control potentials* $\bar{\phi}^e_{ij}$, and R^e_{ij} are their associated rational Bézier functions. R^e_{ij} are the same as are used for the geometry representation. Elements which share geometry control points also share control potentials. The discretisation of Γ and substitution of (11) into (9) gives the 3D IGABEM boundary integral equation,

$$\left[1 - \sum_{e=1}^{E} L^e\right] \phi(\mathbf{p}) + \sum_{e=1}^{E} \sum_{i=0}^{p} \sum_{j=0}^{p} H^e_{ij} \bar{\phi}^e_{ij} = \sum_{e=1}^{E} K^e + \phi^{\text{inc}}(\mathbf{p}), \tag{12}$$

where

$$H^e_{ij} = \int_0^1 \int_0^1 \frac{\partial G(\mathbf{p}, \mathbf{q}_\xi)}{\partial n(\mathbf{q}_\xi)} R^e_{ij}(\xi_1, \xi_2) |J_{\mathbf{F}_e}| \, \mathrm{d}\xi_1 \mathrm{d}\xi_2 - \int_0^1 \int_0^1 \alpha(\mathbf{q}_\xi) G(\mathbf{p}, \mathbf{q}_\xi) R^e_{ij}(\xi_1, \xi_2) |J_{\mathbf{F}_e}| \, \mathrm{d}\xi_1 \mathrm{d}\xi_2, \tag{13}$$

$$L^e = \int_0^1 \int_0^1 \frac{\partial \bar{G}(\mathbf{p}, \mathbf{q}_\xi)}{\partial n(\mathbf{q}_\xi)} \phi(\mathbf{p}) |J_{\mathbf{F}_e}| \, \mathrm{d}\xi_1 \mathrm{d}\xi_2, \tag{14}$$

$$K^e = \int_0^1 \int_0^1 \beta(\mathbf{q}_\xi) G(\mathbf{p}, \mathbf{q}_\xi) |J_{\mathbf{F}_e}| \mathrm{d}\xi_1 \mathrm{d}\xi_2, \tag{15}$$

where $|J_{\mathbf{F}_e}|$ is the Jacobian of the mapping in (10).

2.2.2. Collocation

To find the unknown potentials on Γ, (12) is collocated at a sufficient number of points on the boundary to yield a system of linear equations that can be solved in a conventional fashion. In the conventional BEM, collocation points are placed on element nodes. This is not possible in IGABEM as geometry control points can, and often do, lie off the boundary. Other researchers use the Greville abscissae to collocate on NURBS; however, working with the rational Bézier patches, a $(p+1) \times (p+1)$ grid of points equally spaced in the local (ξ_1, ξ_2) coordinate can be used.

2.3. XIBEM

To form the extended isogeometric BEM, a linear partition-of-unity expansion of plane waves is introduced to express $\bar{\phi}^e_{ij}$ on each basis function such that (11) is reformulated,

$$\phi(\mathbf{q}_\xi) = \sum_{i=0}^{p}\sum_{j=0}^{p} R^e_{i,j}(\xi_1,\xi_2) \sum_{m=1}^{M} A^e_{ijm} \exp\left(\iota k \mathbf{d}^e_{ijm}\cdot\mathbf{q}_\xi\right), \quad \left|\mathbf{d}^e_{ijm}\right| = 1, \quad (16)$$

where there are M plane waves in each expansion with prescribed directions of propagation, $\mathbf{d}^e_{ijm} \in \mathbb{R}^3$, and unknown amplitudes, $A^e_{ijm} \in \mathbb{C}$.

Substitution of (16) into (12) yields

$$\left[1 - \sum_{e=1}^{E} L^e\right]\phi(\mathbf{p}) + \sum_{e=1}^{E}\sum_{i=0}^{p}\sum_{j=0}^{p}\sum_{m=1}^{M} H^e_{ijm} A^e_{ijm} = \sum_{e=1}^{E} K^e + \phi^{\text{inc}}(\mathbf{p}), \quad (17)$$

where L^e and K^e, respectively, are the same as in (14) and (15), and

$$H^e_{ijm} = \int_0^1\int_0^1 \frac{\partial G(\mathbf{p},\mathbf{q}_\xi)}{\partial n} R^e_{ij}(\xi_1,\xi_2)\exp\left(\iota k\mathbf{d}^e_{ijm}\cdot\mathbf{q}_\xi\right)\left|J_{\mathbf{F}_e}\right| \mathrm{d}\xi_1\mathrm{d}\xi_2 - \int_0^1\int_0^1 \frac{\partial \bar{G}(\mathbf{p},\mathbf{q}_\xi)}{\partial n} R^e_{ij}(\xi_1,\xi_2)\exp\left(\iota k\mathbf{d}^e_{ijm}\cdot\mathbf{q}_\xi\right)\left|J_{\mathbf{F}_e}\right| \mathrm{d}\xi_1\mathrm{d}\xi_2, \quad (18)$$

This is the discretised form of the RBIE for 3D XIBEM which can be collocated in order to solve (1). Note that $\phi(\mathbf{p})$ is expressed in a similar fashion to (16):

$$\phi(\mathbf{p}_\xi) = \sum_{i=0}^{p}\sum_{j=0}^{p} R^{e(\mathbf{p})}_{i,j}(\xi_1,\xi_2)\sum_{m=1}^{M} A^{e(\mathbf{p})}_{ijm} e^{\iota k \mathbf{d}^{e(\mathbf{p})}_{ijm}\cdot\mathbf{p}_\xi}, \quad (19)$$

where $\mathbf{p}_\xi \equiv \mathbf{p}(\xi_1,\xi_2)$ and $e(\mathbf{p})$ is the element on which the collocation point $\mathbf{p}$ lies.

2.3.1. Choice of M

The authors use a parameter, τ, as a measure of computational efficiency. τ is defined as the number of degrees of freedom, N_{dof}, divided by the area of the scatterer, Γ, described in term of wavelengths. This can be expressed as

$$\tau = \sqrt{\frac{N_{\text{dof}}}{A_\Gamma/\lambda^2}} = \frac{2\pi}{k}\sqrt{\frac{N_{\text{dof}}}{A_\Gamma}}, \tag{20}$$

where A_Γ is the surface area of the scatterer.

The reader is reminded here of the heuristic requirement for $\tau \geq 10$. It has been shown in two-dimensional XIBEM simulations that this requirement is significantly reduced [24]; this paper will show that this is true for three-dimensional problems also.

In conventional BEM simulations, N_{dof} is typically increased through h- or p-refinement. In IGABEM simulations, corresponding refinements can be made; h-refinements are made through knot refinement of the NURBS surface before decomposition into Bézier patches. XIBEM simulations can use the same refinement techniques as IGABEM but N_{dof} can also be controlled by varying the number of plane waves, M, in the basis enrichment; in this paper, this is referred to as m-refinement. A significant advantage of m-refinement is that the original mesh can be left unchanged, using large elements but many plane waves in the enrichment; thus, XIBEM offers a process that has the potential to entirely circumvent the meshing process by using an identical representation for CAD model and numerical simulation. Other IGA methods require the mesh to be modified (usually refined) as the complexity of the problem increases.

M can be set globally or locally, though the requirement on τ must be

satisfied locally for all Γ_e. It has been found that keeping elements similar in size and using a global value of M provides better system conditioning than a varying local M. Despite this, accurate solutions can be obtained using either approach. As the elements in this work are relatively uniform in size, a global value of M is defined. Bériot *et al.* [31] presented methods of distributing plane waves for geometries that do not have uniformly sized elements.

In two-dimensional simulations, the plane wave directions, $\mathbf{d}^e_{ijm}$, are equally distributed points about the unit-circle. The case in three-dimensions is not as straightforward. The authors adopt the Coulomb Force Method described in [32] to produce an quasi-uniform distribution of wave directions about the unit-sphere. Care is taken so that one of the wave directions is the same as the incident wave propagation direction $\mathbf{d}^{\text{inc}}$ [8]. For problems with multiple incident waves, each direction could be included in the enriched basis; however, poor conditioning of the system matrices may arise if these directions are very similar.

2.3.2. Collocation

The use of a plane wave expansion to multiply each rational Bézier function means that the number of degrees of freedom on each element is greater than the number of control points; thus, a $(p+1) \times (p+1)$ grid of collocation points is no longer sufficient. Instead, a $Z \times Z$ grid of collocation points equally spaced in the local (ξ_1, ξ_2) coordinate system is used on each element, such that the number of collocation points is equal to or greater than the number of degrees of freedom on that element; i.e $Z^2 \geq (p+1)(p+1)M$ (assuming a global M). The scheme can lead to an overdetermined system

matrix; however, this scheme provides an equal spacing of points in the local coordinate and is simple to implement. Also, Peake *et al.* [33] have shown equally spaced points in the local coordinate to be the most effective collocation scheme.

2.4. Integration and solution

For conventional BEM and IGABEM simulations in the numerical examples to follow, a 10×10 Gauss quadrature is used on each element. In order to capture the oscillating function on the large elements used in XIBEM, each of which may span many wavelengths, each element is subdivided into a set of integration cells. If it assumed that each element is square in shape, the number of integration cells is chosen so that the sides of those integration cells are no longer than $\lambda/4$ in length; thus, the number of integration cells, N_{cells}, on an element is expressed as:

$$N_{\text{cells}} = \left\lceil \left(\frac{2k\sqrt{A_e}}{\pi} \right) \right\rceil^2, \tag{21}$$

where $\lceil \cdot \rceil$ denotes the ceiling function[1] and A_e is the area of the element.

To find the potential on Γ, (12) or (17) is evaluated at a set of collocation points. This yields a system of linear equations,

$$\Big[[I - \mathbf{L}]\mathbf{C} + \mathbf{H} \Big] \Big\{ \boldsymbol{\phi} \Big\} = \Big\{ \mathbf{K} + \boldsymbol{\phi}^{\text{inc}} \Big\}, \tag{22}$$

where I is the identity matrix; $\mathbf{L}$ is a diagonal matrix containing the integrals from (14); the matrix $\mathbf{C}$ results from interpolations of $\phi(\mathbf{p})$; the matrix $\mathbf{H}$ is fully populated with integrals from (13) or (18); the vector $\mathbf{K}$ contains

[1] $\lceil x \rceil = \min\{n \in \mathbb{Z} \,|\, n \geq x\}$

the integrals from (15); the vector $\boldsymbol{\phi}^{\text{inc}}$ contains the incident wave potentials at the collocation points; finally, the unknown vector $\boldsymbol{\phi}$ corresponds to the unknown control potentials $\bar{\phi}^e_{ij}$ or amplitudes A^e_{ijm}, depending on whether the simulation is computed using IGABEM or XIBEM.

In order to overcome the non-uniqueness problem, the authors choose to use the technique employed in [3] commonly referred to as the CHIEF method.

Diwan *et al.* [34] have recently suggested that CHIEF is a suitable solution to the non-uniqueness problem and is simpler to implement than dealing with the hyper-singular integrals of the Burton-Miller formulation [4]. In addition to the complex integrals of the Burton-Miller formulation, there is another problem that must be addressed: some NURBS meshes have locations at which control points are coincident (e.g. the poles of a sphere mesh). At these locations, the normal n cannot be calculated, even though it physically exists. These points would typically be used for collocation, which is possible using the conventional BIE or RBIE and CHIEF; conversely, the Burton-Miller formulation requires the normals at collocation points for the hyper-singular equation. If using the Burton-Miller formulation, these collocation points have to be adjusted as in [23].

The introduction of the partition-of-unity enrichment leads to ill-conditioned matrices. Therefore, the system in (22) is solved using singular value decomposition (SVD). Though this is not necessary in all cases—the conditioning of some matrices is suitable for a QR decomposition—SVD provides a highly accurate solution from the BEM equations.

3. Numerical results

In this paper, three types of BEM simulation are referred to: *conventional BEM* implies a piecewise, polynomial BEM using continuous, isoparametric, quadratic elements; *IGABEM* implies an isogeometric BEM using the rational Bézier functions of a decomposed NURBS surface to describe the geometry and potential function over the scatterer; *XIBEM* refers to the extended isogeometric BEM.

Unless stated otherwise, all the errors $\mathcal{E}$ are evaluated in a relative L^2-norm sense,

$$\mathcal{E} = \frac{\left\|\phi - \phi^{\text{ref}}\right\|_{L^2(\Gamma)}}{\left\|\phi^{\text{ref}}\right\|_{L^2(\Gamma)}} \tag{23}$$

where ϕ represents the total potential (scattered plus incident) on the surface of the scatterer, evaluated by numerical simulation; ϕ^{ref} is a reference solution calculated using an analytical solution or approximated from a converged reference solution. Both sets of potentials are calculated at equally spaced points (at least 1000) over Γ so that the norms can be calculated in a trapezoidal rule sense.

3.1. Unit sphere

The first problem considered is a plane wave impinging a perfectly reflecting sphere, i.e. the boundary condition $\alpha(\mathbf{q}) = \beta(\mathbf{q}) = 0$. The sphere has radius $a = 1$; the incident wave is of unit amplitude and propagates in the direction $\mathbf{d}^{\text{inc}} = (1, 0, 0)$. The scattered acoustic potential ϕ^{scat} can be found at any point $\mathbf{x}(r, \theta)$ with an analytical solution [35]. θ is the azimuthal; the polar coordinate is not required as it is an axisymmetric problem. The

analytical solution defined:

$$\phi^{\text{scat}}(r,\theta) = \sum_{n=0}^{\infty} -\frac{\iota^n(2n+1)j_n'(ka)}{h_n'(ka)} P_n(\cos\theta) h_n(kr) \tag{24}$$

where j_n is the spherical Bessel function of the first kind, a prime denotes its derivative, h_n is the spherical Hankel function of the first kind, and P_n is the Legendre function of the first kind. The total wave potential at $\mathbf{x}(r,\theta)$ is the sum of the incident and scattered potential: $\phi = \phi^{\text{inc}} + \phi^{\text{scat}}$.

For the conventional BEM mesh, the cube-to-sphere mapping described in [32] is used. The sphere is discretised initially into six elements. These six elements are the faces of a cube with coordinates $\bar{x}, \bar{y}, \bar{z} \in [-1,1]^3$, mapped on the surface of the sphere. The points on the sphere (x,y,z) are found with the mapping

$$\begin{aligned} x &= \bar{x}\sqrt{1 - \frac{\bar{y}^2}{2} - \frac{\bar{z}^2}{2} + \frac{\bar{y}^2\bar{z}^2}{3}}, \\ y &= \bar{y}\sqrt{1 - \frac{\bar{x}^2}{2} - \frac{\bar{z}^2}{2} + \frac{\bar{x}^2\bar{z}^2}{3}}, \\ z &= \bar{z}\sqrt{1 - \frac{\bar{x}^2}{2} - \frac{\bar{y}^2}{2} + \frac{\bar{x}^2\bar{y}^2}{3}}. \end{aligned} \tag{25}$$

A sphere meshed using this mapping can be seen in Figure 1. To refine this mesh, each element is simply split into a square number $(4, 9, 16, \ldots)$ of smaller elements; a refined meshed is seen in Figure 2.

The initial IGABEM and XIBEM meshes are created by rotating a semi-circular arc about a central axis—in this case, the z-axis is used. The initial mesh can be seen in Figure 3, with control points that lie off the surface of the sphere clearly visible. Figure 3 is the final mesh for XIBEM; the rational Bézier functions of each geometry element can simply be enriched.

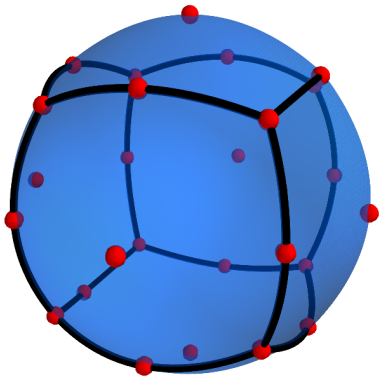

Figure 1: Conventional BEM sphere mesh: initial cube-to-sphere mesh with six elements.

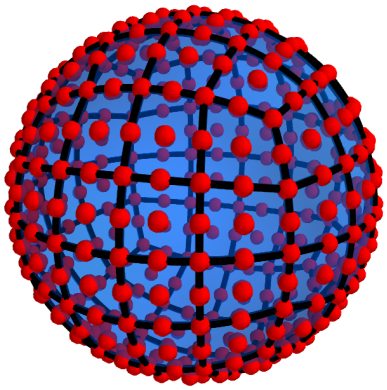

Figure 2: Conventional BEM sphere mesh: h-refined mesh; each face has been split into sixteen elements.

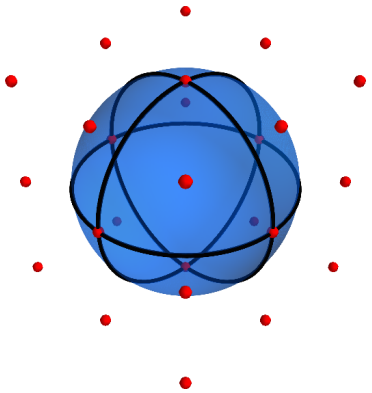

Figure 3: Representation of NURBS-based mesh: initial mesh for IGABEM and XIBEM.

For IGABEM, refinements can be made through knot insertion; this is similar to how the elements are split for the conventional BEM. The refined mesh can be seen in Figure 4. From visual examination, the refined IGABEM mesh is not as regular as the mesh in Figure 2. Despite this, it will be shown that the exact geometry used for integration and the rational Bézier functions used to approximate the potential over the surface of the scatterer provide a similarly accurate solution.

Another immediate difference that is apparent between the conventional BEM meshes and this isogeometric mesh is the shape of the elements: the mesh in Figure 3 has seemingly triangular elements. These elements are, in fact, collapsed quadrilaterals; the three points along one edge are simply coincident. In this case, these points are the north and south pole of the sphere. For the purposes of functional approximation, the degrees of freedom at these coincident control points are considered a single degree of freedom.

At the poles, the normal n cannot be calculated because the Jacobian is undefined. This is not a problem for the formulation used in this work as no

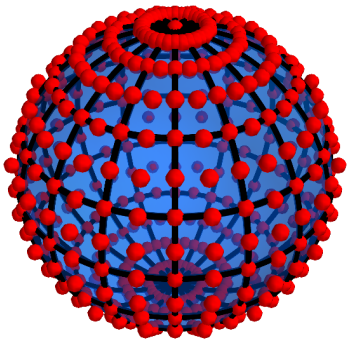

Figure 4: Representation of NURBS-based mesh: refined mesh for IGABEM; note the pole at the top and bottom.

integration points are placed there; however, assuming collocation points are placed there, the Burton-Miller formulation would require derivatives at this point and so manual adjustments are required for analysis [23]. Although the analytical value of n at the poles could be included in the current code, the scope of the current work is to create a generic method. This makes the use of CHIEF points rather than the Burton-Miller formulation more desirable when using isogeometric meshes for acoustic scattering analysis.

Using the $Z \times Z$ collocation grid, described in the formulation, will give multiple collocation points at the poles. As only one of these equations can be used—the rest providing no additional information—there will be an insufficient number of collocation points. Therefore, a $(Z+1) \times (Z+1)$ grid is used (to ensure an adequate number of equations) with the coincident collocation points replaced by a single collocation point.

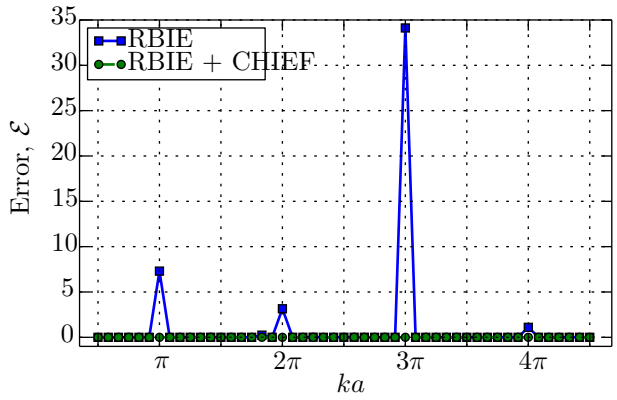

Figure 5: Comparison of L_2 errors $\mathcal{E}$ of XIBEM simulations of the unit sphere problem with $M = 50$.

3.1.1. CHIEF

A demonstration of the efficacy of CHIEF to overcome the nonuniqueness problem is now given. For a sphere of radius a, the eigenfrequencies at which nonuniqueness occurs are those corresponding to $ka = n\pi$ where $n \in \mathbb{Z}^+$. To demonstrate the effect of CHIEF points, two sets of XIBEM simulations were run over a range of wavenumbers using 50 plane waves in the basis enrichment; one set of simulations used only collocation points on the surface of the scatterer while the other set the other set considered an additional five CHIEF collocation points (an arbitrary but small number). The error of each simulation was evaluated using (23) and (24). The results can be seen in Figure 5. The results verify that the XIBEM formulation with CHIEF is stable at the irregular frequencies while simulations without CHIEF are clearly unstable at those frequencies.

3.1.2. Determining $\boldsymbol{\tau}$ required

The number of degrees of freedom N_{dof} used in a BEM simulation has a direct and significant impact on the runtime of that simulation. It is, therefore, desirable to use as few degrees of freedom as possible whilst not compromising on solution accuracy. The reader is reminded that, in this work, the measure of computational efficiency is τ, defined as the number of degrees of freedom per wavelength in each coordinate direction. For the unit sphere, this can be explicitly expressed as

$$\tau = \frac{1}{k}\sqrt{\pi N_{\text{dof}}}. \tag{26}$$

It is desirable to use a method that requires only a low τ to provide results of the required accuracy.

Simulations of the unit-sphere problem are run over a spectrum. Starting with the coarsest mesh and adding more degrees of freedom through h-refinement (for conventional BEM or IGABEM) or adding plane waves into the enriched basis (XIBEM), simulations are stopped when the error of that simulation is $\leq 1\%$. Figure 6 shows the N_{dof} required for a solution of accuracy $\mathcal{E} \leq 1\%$. Figure 7 shows the values of τ calculated using (26) and the data from Figure 6.

It is prudent to note that the simulations are confined to the meshes defined at the start of this section and shown in Figures 1–4. Due to the way the refinements are being made, there are significant jumps in N_{dof} at each refinement level. Table 1 notes the first few of these refinement levels for the meshes used. The XIBEM mesh consists of the 26 rational Bézier functions of the first IGABEM mesh multiplied by the plane wave enrichments; the N_{dof} of the XIBEM mesh is simply then $26M$.

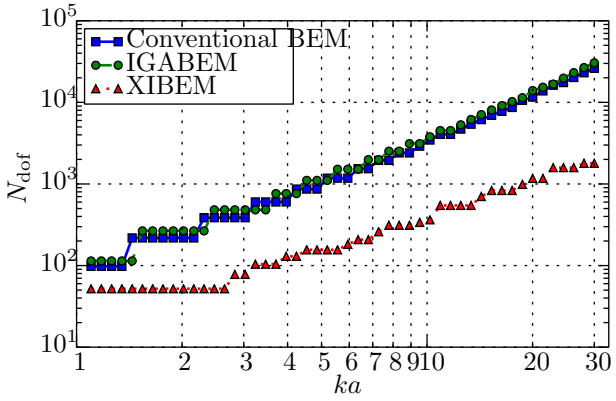

Figure 6: Number of degrees of freedom required to obtain 1% error with conventional BEM, IGABEM and XIBEM simulations over a range of wavenumbers.

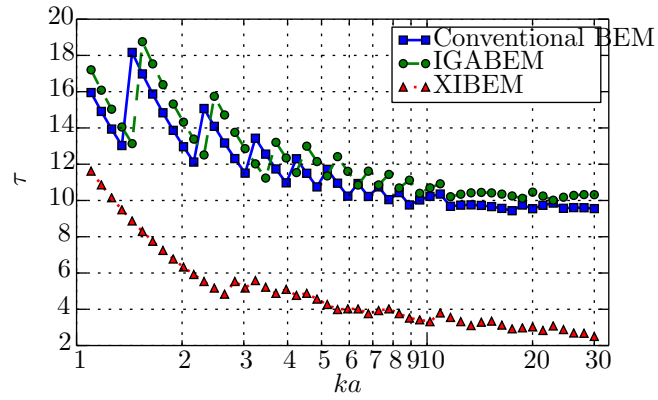

Figure 7: τ required to obtain 1% error with conventional BEM, IGABEM and XIBEM simulations over a range of wavenumbers.

Table 1: Conventional BEM and IGABEM mesh data for the scattering sphere problem

	Conventional BEM					IGABEM					XIBEM				
Refinement level	1	2	3	4	5	1	2	3	4	5	1	2	3	4	5
E	6	24	54	96	150	8	32	72	128	200	8	8	8	8	8
N_{dof}	26	98	21	386	602	26	114	266	482	762	26	52	78	104	130

Taking the above into consideration, the results for low ka in Figures 6 and 7 do not show the minimum N_{dof} and τ required for any conventional BEM/IGABEM/XIBEM simulation of this problem, but rather those of simulations using the meshes defined in this section. This explains the plateaus seen in the plots of Figure 6 and helps to understand the seemingly high values of τ seen for low ka in Figure 7. The step changes in τ seen in the latter figure correspond to the step changes in N_{dof}.

Despite the above, there is a clear trend seen in Figure 7: XIBEM simulations require fewer degrees of freedom than both conventional BEM and IGABEM simulations. As ka increases, conventional BEM and IGABEM simulations appear to need $\tau \approx 10$ for a 1% error while XIBEM simulations require $\tau \approx 3$.

Finally for this set of simulations, the condition numbers of the system matrices can be seen in Figure 8. In previous two-dimensional work [24, 33, 36], it was observed that the approximation basis enrichment had a strong detrimental effect on the conditioning of the system matrices: condition numbers $> 10^{16}$ were recorded. Despite these high condition numbers, solving these systems with SVD still provided very accurate solutions. In Figure 8, higher condition numbers are observed for XIBEM again; however, the conditioning in this three-dimensional problem is far better than seen in the equivalent two-dimensional problem. This is possibly due to the enrichment functions—the plane waves—being more sparsely oriented in three dimensions instead of two.

As the condition numbers are lower, more efficient solvers could potentially be used. However, the runtimes of simulations are dominated by the

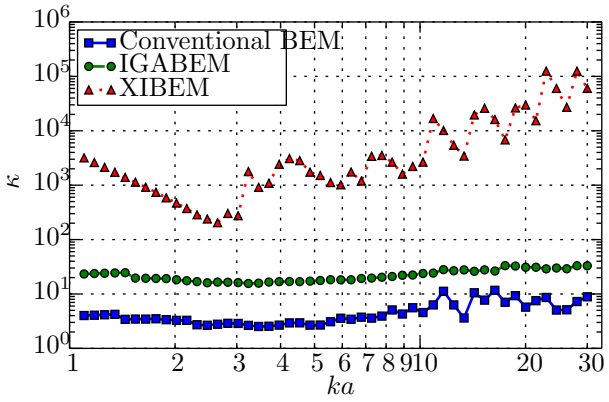

Figure 8: Conditioning of system matrices of simulations in Figure 6.

integration and building of the system matrices. This took at least 97% of the total runtime of all XIBEM simulations (it took 99% on average).

3.1.3. Medium wavelength problems

While the previous results show the comparative performance of XIBEM against conventional BEM and IGABEM schemes, the main interest of the work lies in solving problems of shorter wavelengths. By reducing the N_{dof} required to solve a certain problem to a given accuracy, this extends the spectrum for which accurate results can be obtained with a fixed computational resource. The conventional BEM and IGABEM problems in Figures 6–8 were the largest that could be solved on the conventional desktop PC used for this work, with the largest system matrix being $10,686 \times 10,586$ (approximately 1.8 GB of memory with complex double precision).

XIBEM simulations are run over the spectrum $ka \in [20, 60]$, adjusting M such that $\tau \approx 3$. The errors of these simulations can be seen in Figure 9 and the condition numbers in Figure 10. For $ka = 60$, the number of plane waves was $M = 396$ and the system matrix was $10,396 \times 10,296$ in size. The

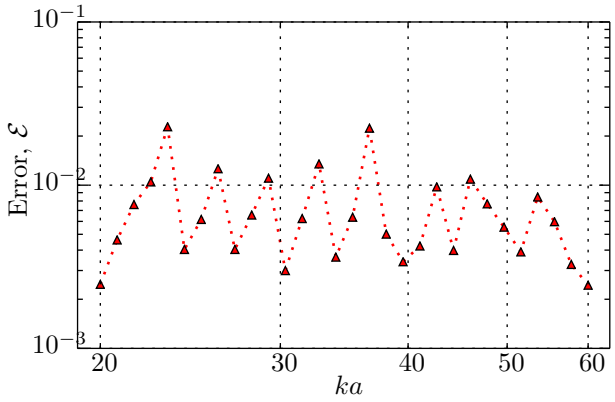

Figure 9: L^2 errors, $\mathcal{E}$, of XIBEM simulations of medium wavelength simulations of unit-sphere problem.

conditioning of the system matrices is degrading at higher k; this is caused by the higher M required to maintain$\tau \approx 3$. Despite this, SVD is obtaining a good solution as it does in the two-dimensional case.

3.1.4. Off-surface wave potential

The results displayed so far relate to the total potential on the surface of the scatterer. However, engineers are equally, if not more, interested in the wave potential off the scatterer. It is found that the errors in BEM approximations of potential off the surface of a scatterer are lower than those found on the surface. This is due to the smoothing effect of the integration in the BIE; on the surface of a scatterer, the potential is simply found through interpolation of the basis on each element. Table 2 displays some errors of IGABEM and XIBEM simulations on and off the surface of the unit sphere. The off-surface errors were calculated by evaluating the potential at points on the surface of an imaginary sphere of radius $a = 5$. The increase in accuracy when evaluating potentials off-surface is clear.

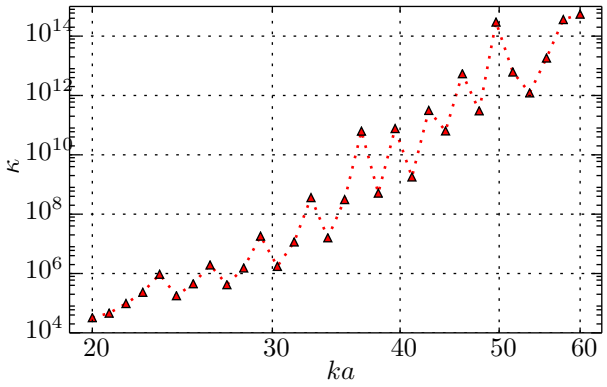

Figure 10: Condition numbers, κ, of XIBEM simulations of medium wavelength simulations of unit-sphere problem.

Table 2: Difference between L^2 errors evaluated on the surface of the spherical scatterer and in the far field.

	IGABEM			XIBEM		
	N_{dof}	L^2 surface	L^2 off-surface	N_{dof}	L^2 surface	L^2 off-surface
$ka = 3$	482	7.0×10^{-3}	1.4×10^{-4}	78	6.9×10^{-3}	1.7×10^{-4}
$ka = 7.75$	1986	1.1×10^{-2}	3.7×10^{-4}	260	1.5×10^{-2}	1.3×10^{-3}
$ka = 20$	13946	9.2×10^{-3}	9.5×10^{-4}	1170	5.0×10^{-3}	7.8×10^{-4}

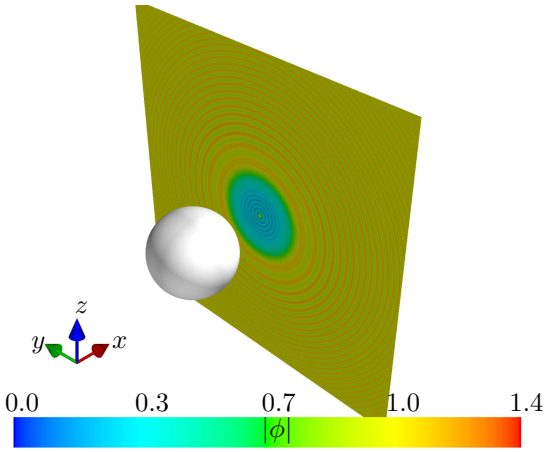

Figure 11: Total scattered wave in the unit-sphere problem; $x = 2$ plane; ka=60.

Figure 11 is a plot of absolute total potential, off the surface of the sphere, obtained using an XIBEM simulation.

3.2. Torus

The next problem to be examined is that of a scattering torus. Simulations are run for the cases of an impinging wave propagating in the direction $\mathbf{d}^{\text{inc}} = \left(\frac{3}{5}, 0, -\frac{4}{5}\right)$. The torus specified here is a ring torus with major radius $R = 1$ and minor radius $r = 0.5$. The geometry of the torus is shown in Figure 12.

The reason for including this example is that it is a problem that cannot be solved using conventional BEM or IGABEM on a desktop PC due to the number of degrees of freedom required to obtain an accurate solution.

The isogeometric representation of the torus mesh is shown in Figure 13 and 14. It consists of 32 elements and 128 control points. Unlike the sphere, the isogeometric representation of a torus does not have any polar

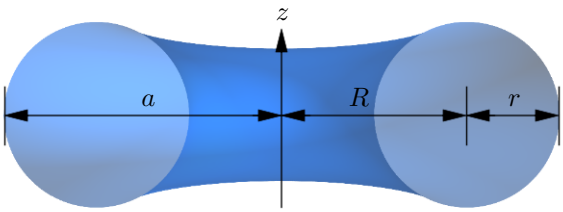

Figure 12: Slice of torus geometry at $y = 0$. The torus appears to be slender in the middle due to the perspective used.

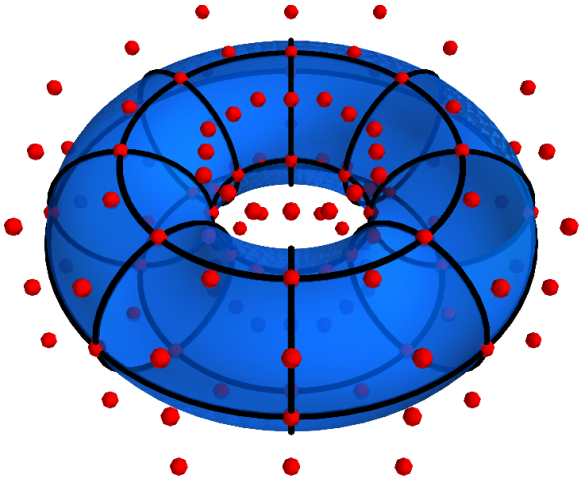

Figure 13: Torus mesh: isometric view.

singularities. The surface area of a torus is $4\pi^2 Rr$, so this torus has a surface area of $2\pi^2$; the parameter τ for this geometry is therefore defined as

$$\tau = \frac{2\pi}{k}\sqrt{\frac{N_{\text{dof}}}{A_\Gamma}} = \frac{1}{k}\sqrt{2N_{\text{dof}}}. \tag{27}$$

Two cases are considered: the first is $ka = 30$; the second is $ka = 45$. Note that $a = R + r = 1.5$. There is no analytical solution for this problem and so a converged Method of Fundamental Solutions (MFS) [37] solution is used to evaluate the errors in the approximation. Using a conventional BEM (with $\tau = 10$), these simulations would require $20,000$ and $45,000$ degrees

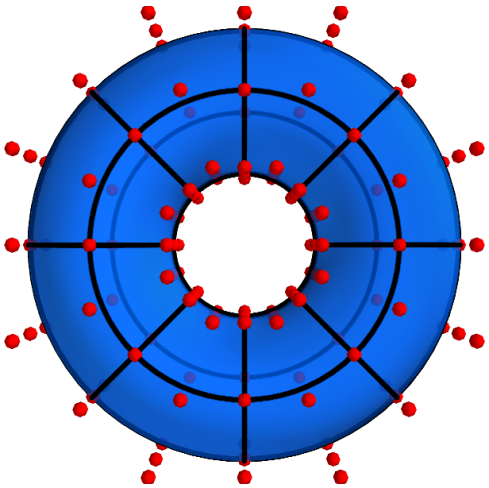

Figure 14: Torus mesh: view along the z-axis.

of freedom respectively; the latter of these two would then require a 32 GB matrix to be stored and inverted. For this reason, only XIBEM and PU-BEM simulations of this problem are run. The PU-BEM solution is possible due to the torus geometry having the analytical parametric representation:

$$x = (R + r\cos\theta_2)\cos\theta_1, \tag{28}$$

$$y = (R + r\cos\theta_2)\sin\theta_1, \tag{29}$$

$$z = r\sin\theta_2, \tag{30}$$

where $\theta_1, \theta_2 \in [0, 2\pi)$. The PU-BEM mesh has the same element shapes as the XIBEM mesh so that the results are comparable.

Initial tabulated results of XIBEM and PU-BEM simulations can be found in Table 3. The L^2-errors were evaluated by comparing the potential at 2,592 points, equally spaced over the local coordinate of each element on the torus. The table shows that XIBEM and PU-BEM accuracies are comparable, with neither method providing consistently more accurate ap-

Table 3: Initial tabulated results of simulations of torus problem with $ka = 30$.

			XIBEM		PU-BEM	
M	N_{dof}	τ	κ	$L^2(\Gamma)$ error	κ	$L^2(\Gamma)$ error
13	1,664	2.88	3.7×10^3	6.35%	2.8×10^3	9.42%
16	2,048	3.20	6.3×10^3	2.36%	5.5×10^3	1.53%
19	2,432	3.49	3.2×10^4	1.01%	3.1×10^4	1.46%
22	2,816	3.75	4.0×10^5	1.86%	3.8×10^5	1.69%
25	3,200	4.00	2.1×10^5	0.18%	2.6×10^5	0.22%

proximations. However, it should be noted again that the PU-BEM simulations are only possible because of the available parametric equations in (28)–(30); without this analytical representation, PU-BEM would not provide the saving in degrees of freedom that the XIBEM does.

It is interesting to see that the errors in Table 3 do not decrease uniformly: in particular, there is a significant reduction in errors between the first two rows and the last two rows. The reason for these reductions is the large increase in the number of collocation points being used. For the $M = 13$ simulations, 2,048 collocation points are used; for the $M = 16, 19, 22$, simulations, 3,200 collocation points are used; for the $M = 25$ simulations, 4,608 collocation points are used. Clearly, the number of collocation points has an impact on the solution accuracy. This was not an observation made for the sphere problem as there was already an excess of collocation points from the $(Z + 1) \times (Z + 1)$ grid.

Table 4 shows some errors and condition numbers of XIBEM simulations

Table 4: Comparison of errors and system condition number of XIBEM simulations of torus problem ($ka = 30$) with varying numbers of collocation points.

$M = 19$				$M = 22$			
N_{coll}	$\frac{N_{\text{coll}}}{N_{\text{dof}}}$	κ	L^2 error	N_{coll}	$\frac{N_{\text{coll}}}{N_{\text{dof}}}$	κ	L^2 error
2,592	1.07	2.5×10^5	3.33%	3,200	1.14	3.8×10^5	1.33%
3,200	1.32	3.4×10^4	1.09%	3,872	1.38	8.0×10^4	0.49%
3,872	1.59	1.8×10^4	0.66%	4,608	1.64	5.2×10^4	0.32%
4,608	1.89	1.4×10^4	0.43%	5,408	1.92	4.4×10^4	0.18%
5,408	2.22	1.4×10^4	0.47%	6,272	2.23	4.1×10^4	0.16%

of the torus problem using different numbers of collocation points, N_{coll}. These are displayed along with the fraction of collocation points to degrees of freedom. As the number of collocation points used increases, the error decreases. This effect is significant for $N_{\text{coll}}/N_{\text{dof}} < 1.5$; it appears less significant for greater values. The effect can also be noted in the condition numbers of the system that fall as the system becomes increasingly over-determined.

As the collocation scheme used in this 3D work is fixed to a square grid of points, it is not possible to determine with any certainty what fraction of $N_{\text{coll}}/N_{\text{dof}}$ is ideal. Indeed, it could be the case that this fraction is not constant. It is also possible that a rectangular grid could be more suitable given that the elements along the major radius of the torus of the outermost of the torus appear rectangular; this type of grid would also give more control of the number of collocation points used.

XIBEM and PU-BEM simulations were also run of the torus problem

Table 5: Initial tabulated results of XIBEM simulations of torus problem with $ka = 45$.

					XIBEM		PU-BEM	
M	N_{dof}	N_{coll}	$\frac{N_{\text{coll}}}{N_{\text{dof}}}$	τ	κ	L^2 error	κ	L^2 error
28	3,584	5,408	1.51	2.82	1.0×10^4	3.66%	8.2×10^3	3.15%
34	4,352	6,272	1.44	3.11	5.0×10^4	1.13%	4.9×10^4	1.51%
41	5,248	8,192	1.56	3.41	2.4×10^5	0.28%	2.6×10^5	0.39%
49	6,272	9,248	1.47	3.73	2.3×10^6	0.15%	2.7×10^6	0.27%
57	7,296	11,552	1.58	4.03	1.4×10^7	0.06%	1.5×10^7	0.09%

with a shorter wavelength: $ka = 45$. The results of the simulations can be seen in Table 5. Care was taken so that at least 1.4 times as many collocation points were used as degrees of freedom. By doing this, the errors continue to decrease as τ is increased; this is more like the behaviour expected of both the PU-BEM and XIBEM and observed in earlier works [24, 32, 33].

Four of the five simulations in Table 5 show XIBEM to give a more accurate approximation than PU-BEM. However, the values are similar and four simulations is not enough to claim a statistical significance. The system condition numbers of both approaches are similar too, showing that the plane wave enrichment is the main cause of ill conditioning. None of the condition numbers is significantly large; however, they are greater than those found for $ka = 30$.

The performance of XIBEM and PU-BEM are, as expected, comparable. It should be reiterated, however, that this is a special case for which PU-BEM is easily implemented due to the analytical parametric representation

of a torus. While it may be possible to provide an analytical geometry to PU-BEM for more complex problems, this task becomes increasingly more difficult with increasingly complex geometries. Conversely, the analytical geometry is a property inherent in the use of XIBEM as the geometry functions can be imported directly from a CAD model. So while, XIBEM and PU-BEM perform similarly for problems that may be compared, there may be some more complex problems for which PU-BEM cannot be used as easily.

Using more collocation points reduces the benefits that the PU-BEM and XIBEM have over conventional BEM simulations in that the total number of matrix entries increases. However, the benefit of the reduction in N_{dof} is still significant. Consider the case of $ka = 45$ using a conventional BEM simulation. For a 1% error, this would require $\tau \approx 10$ or 45,000 degrees of freedom; this gives a matrix system with over 2 billion complex coefficients. Conversely, considering the case of $\tau = 3.41$ in Table 5, the matrix system has approximately 43 million entries. This is almost a 98% reduction in matrix entries, a significant saving.

Figure 15 is a plot of potential on the torus surface. Figures 16 and 17 are plot of scattering off the torus surface; Figure 16, in particular, shows the internal reflections created within the torus. The figures show the short wavelength of the problem being solved.

4. Conclusions

Decomposed NURBS meshes have been used to represent the geometries of three-dimensional scatterers. The functions that describe these geometries, multiplied by families of plane waves, have been used to approximate

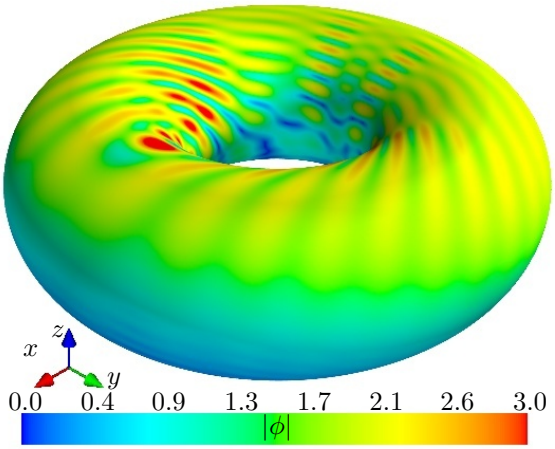

Figure 15: Isometric view of absolute total field on the torus; ka=45.

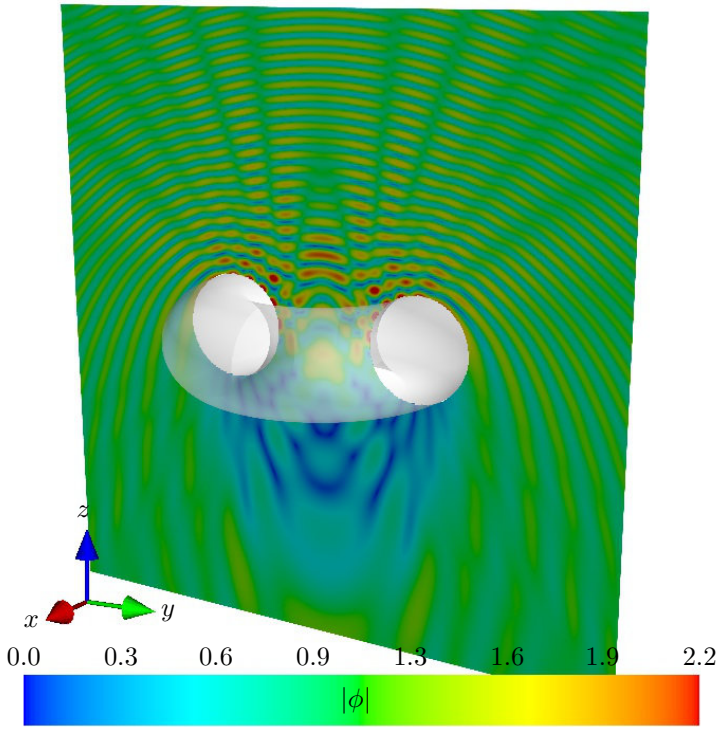

Figure 16: $x = 0$ plane of absolute value of total field of the torus problem; ka=45.

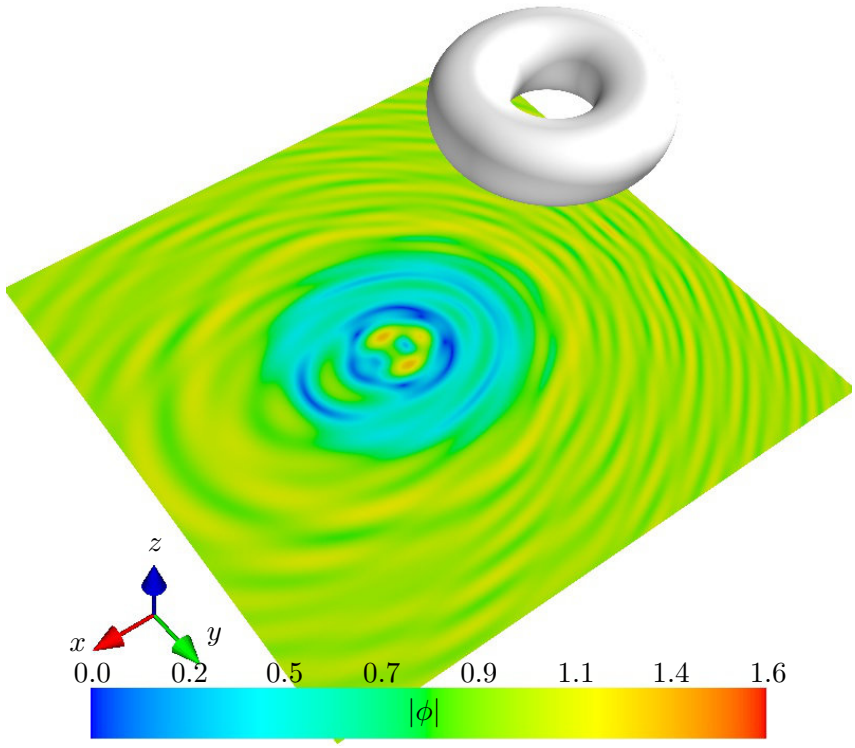

Figure 17: Absolute value of total acoustic field of the torus problem shown at $z = -3$; ka=45.

the potential over the surface of the scatterers. Using this discretisation in a direct collocation BEM approach, the so-called extended isogeometric boundary element method, has given accurate approximations.

Compared to the PU-BEM, the XIBEM performs similarly with neither method appearing significantly more accurate. However, the XIBEM has an analytical geometry provided by the same functions used in approximation of the field variable. The problems explored in this paper were both special cases for which there is an easy analytical geometry representation for PU-BEM.

In the example of a scattering sphere used in this paper, IGABEM has not been shown to be more accurate than the conventional BEM when using the same number of degrees of freedom. Meshing may be easier with an isogeometric mesh but the basis functions take longer to evaluate and so it is undesirable to use unless there is an accuracy benefit also.

The previous comment is not conclusive. The results shown in this paper are for one problem. That problem is solved used a decomposed NURBS mesh. The decomposed mesh consists of C^0 patches while the original mesh has a higher continuity. It is expected that this has a negative impact on IGABEM simulation. In previous work by the authors (and by other authors) IGABEM simulations using the original NURBS mesh have consistently demonstrated better performance compared to BEM simulations using Lagrangian polynomials; therefore, it could be argued that the comparison made here is not fair. Further investigations into the effect on IGABEM of using Bézier decomposition are required; this should be done for multiple geometries. Again, the authors note that the choice of using Bézier decom-

position was for ease of implementation in existing code.

Conversely, in this same example, the XIBEM requires far fewer degrees of freedom to achieve engineering accuracy for the same problem. Although the XIBEM requires a surplus of collocation points to obtain the greatest accuracy, the overall reduction in matrix size is significant, approaching 98%.

XIBEM still requires a more efficient integration scheme to compete with the acceleration methods that can be applied to conventional BEM and IGA-BEM. The nature of the optimal collocation scheme is still be understood also. Despite this, XIBEM is clearly a method that has significant potential and is deserving of more research.

References

[1] R. P. Banaugh, W. Goldsmith, Diffraction of steady acoustic waves by surfaces of arbitrary shape, Journal of the Acoustical Society of America 35 (1963) 1590–1601.

[2] L. G. Copley, Fundamental results concerning integral representations in acoustic radiation, Journal of the Acoustical Society of America 44 (1963) 28–32.

[3] H. A. Schenck, Improved integral formulation for acoustic radiation problems, Journal of the Acoustical Society of America 44 (1968) 41–58.

[4] A. J. Burton, G. F. Miller, The application of integral equation methods to the numerical solution of some exterior boundary-value problems, Proceedings of the Royal Society of London. A. 323 (1971) 201–210.

[5] P. Bettess, Short-wave scattering: problems and techniques, Philosophical Transactions of the Royal Society A—Mathematical, Physical & Engineering Sciences 362 (2004) 421–443.

[6] J. M. Melenk, I. Babuška, The partition of unity finite element method: Basic theory and applications, Computer Methods in Applied Mechanics and Engineering 139 (1996) 289–314.

[7] H. Bériot, E. Perrey-Debain, M. Ben Tahar, C. Vayssade, Plane wave basis in Galerkin BEM for bidimensional wave scattering, Engineering Analysis with Boundary Elements 34 (2010) 130–143.

[8] E. Perrey-Debain, O. Laghrouche, P. Bettess, J. Trevelyan, Plane-wave basis finite elements and boundary elements for three-dimensional wave scattering, Philosophical Transactions of the Royal Society of London. Series A: Mathematical, Physical & Engineering Sciences 362 (2004) 561–577.

[9] P. Massimi, R. Tezaur, C. Farhat, A discontinuous enrichment method for three-dimensional multiscale harmonic wave propagation problems in multi-fluid and fluid-solid media, International Journal for Numerical Methods in Engineering 76 (2008) 400–425.

[10] L. Kovalevsky, P. Ladevèze, H. Riou, M. Bonnet, The variational theory of complex rays for three-dimensional Helmholtz problems, Journal of Computational Acoustics 20 (2012) 1250021.

[11] T. Luostari, T. Huttunen, P. Monk, Error estimates for the ultra weak

variational formulation in linear elasticity, ESAIM: Mathematical Modelling and Numerical Analysis 47 (2013) 183–211.

[12] T. J. R. Hughes, J. A. Cottrell, Y. Bazilevs, Isogeometric analysis: CAD, finite elements, NURBS, exact geometry and mesh refinement, Computer Methods in Applied Mechanics and Engineering 194 (2005) 4135–4195.

[13] J. J. S. P. Cabral, L. C. Wrobel, C. A. Brebbia, A BEM formulation using B-splines: I-uniform blending functions, Engineering Analysis with Boundary Elements 7 (1990) 136–144.

[14] J. J. S. P. Cabral, L. C. Wrobel, C. A. Brebbia, A BEM formulation using B-splines: II-multiple knots and non-uniform blending functions, Engineering Analysis with Boundary Elements 8 (1991) 51–55.

[15] C. Politis, A. I. Ginnis, P. D. Kaklis, K. Belibassakis, C. Feurer, An isogeometric BEM for exterior potential-flow problems in the plane, in: 2009 SIAM/ACM Joint Conference on Geometric and Physical Modeling, SPM '09, ACM, New York, NY, USA, 2009, pp. 349–354.

[16] L. Kang, X. Qian, Isogeometric analysis and shape optimization via boundary integral, Computer-Aided Design 43 (2011) 1427–1437.

[17] R. N. Simpson, S. P. A. Bordas, J. Trevelyan, T. Rabczuk, A two-dimensional isogeometric boundary element method for elastostatic analysis, Computer Methods in Applied Mechanics and Engineering 209-212 (2012) 87–100.

[18] R. N. Simpson, S. P. A. Bordas, H. Lian, J. Trevelyan, An isogeometric boundary element method for elastostatic analysis: 2D implementation aspects, Computers & Structures 118 (2013) 2–12.

[19] T. Takahashi, T. Matsumoto, An application of fast multipole method to isogeometric boundary element method for Laplace equation in two dimensions, Engineering Analysis with Boundary Elements 36 (2012) 1766–1775.

[20] M. A. Scott, R. N. Simpson, J. A. Evans, S. Lipton, S. P. A. Bordas, T. J. R. Hughes, T. W. Sederberg, Isogeometric boundary element analysis using unstructured T-splines, Computer Methods in Applied Mechanics and Engineering 254 (2013) 197–221.

[21] K. A. Belibassakisa, K. V. Gerostathisb, Th P. Kostasb, C. G. Politis, P. D. Kaklisa, A. I. Ginnisa, C. Feurera, A BEM-isogeometric method for the ship wave-resistance problem, Ocean Engineering 60 (2013) 53–67.

[22] L. Heltai, M. Arroyo, A. DeSimone, Nonsingular isogeometric boundary element method for Stokes flows in 3D, Computer Methods in Applied Mechanics and Engineering 268 (2014) 514–539.

[23] R. N. Simpson, M. A. Scott, M. Taus, D. C. Thomas, H. Lian, Acoustic isogeometric boundary element analysis, Computer Methods in Applied Mechanics and Engineering (2013).

[24] M. J. Peake, J. Trevelyan, G. Coates, Extended isogeometric boundary element method (XIBEM) for two-dimensional Helmholtz problems,

Computer Methods in Applied Mechanics and Engineering 259 (2013) 93–102.

[25] L. C. Wrobel, The Boundary Element Method, Vol. I: Applications in Thermo-fluids and Acoustics, John Wiley & Sons, Ltd., Chichester, UK, 2002.

[26] Y. Liu, Fast Multipole Boundary Element Method: Theory and Applications in Engineering, Cambridge University Press, 2009.

[27] J. J. Rêgo Silva, L. C. Wrobel, J. C. F. Telles, A new family of continuous/discontinuous three-dimensional boundary elements with application to acoustic wave propagation, International Journal for Numerical Methods in Engineering 36 (1993) 1661–1679.

[28] Y. Bazilevs, V. M. Calo, J. A. Cottrell, J. A. Evans, T. J. R. Hughes, S. Lipton, M. A. Scott, T. W. Sederberg, Isogeometric analysis using T-splines, Computer Methods in Applied Mechanics and Engineering 199 (2010) 229–263.

[29] L. Piegl, W. Tiller, The NURBS book, Springer-Verlag, 2nd edition, 1997.

[30] M. J. Borden, M. A. Scott, J. A. Evans, T. J. R. Hughes, Isogeometric finite element data structures based on Bézier extraction of NURBS, International Journal for Numerical Methods in Engineering 87 (2011) 15–47.

[31] H. Bériot, E. Perrey-Debain, M. Ben Tahar, C. Vayssade, On a Galerkin

wave boundary element formulation for scattering by non-smooth obstacles, in: Proceedings of 8th International Conference on Mathematical and Numerical Aspects of Waves, pp. 400–402.

[32] M. J. Peake, J. Trevelyan, G. Coates, The equal spacing of n points on a sphere with application to partition-of-unity wave diffraction problems, Engineering Analysis with Boundary Elements 40 (2014) 114–122.

[33] M. J. Peake, J. Trevelyan, G. Coates, Novel basis functions for the partition of unity boundary element method for Helmholtz problems, International Journal for Numerical Methods in Engineering 93 (2013) 905–918.

[34] G. C. Diwan, J. Trevelyan, G. Coates, A comparison of techniques for overcoming non-uniqueness of boundary integral equations for the collocation partition of unity method in two-dimensional acoustic scattering, International Journal for Numerical Methods in Engineering 96 (2013) 645–664.

[35] P. M. Morse, H. Feshbach, Methods of Theoretical Physics: Part II, McGraw-Hill, 1953.

[36] E. Perrey-Debain, J. Trevelyan, P. Bettess, Plane wave interpolation in direct collocation boundary element method for radiation and wave scattering: numerical aspects and applications, Journal of Sound and Vibration 261 (2003) 839–858.

[37] P. S. Kondapalli, D. J. Shippy, G. Fairweather, Analysis of acoustic

scattering in fluids and solids by the method of fundamental solutions, Journal of the Acoustical Society of America 91 (1992) 1844–1854.